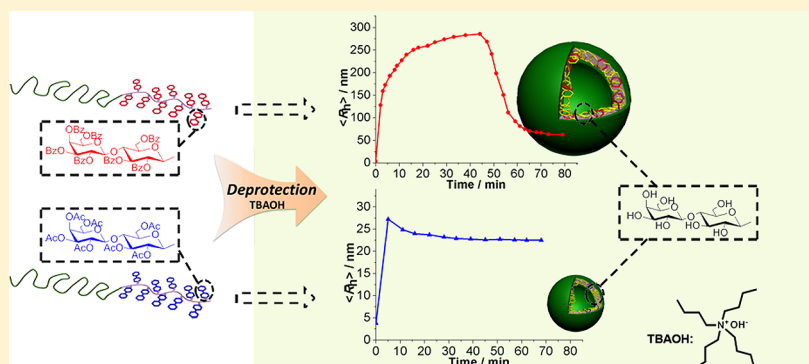# Deprotection-Induced Micellization of Glycopolymers: Control of Kinetics and Morphologies

Xiulong Wu, Lu Su, Guosong Chen,* and Ming Jiang

The State Key Laboratory of Molecular Engineering of Polymers, Collaborative Innovation Center of Polymers and Polymer Composite Materials and Department of Macromolecular Science, Fudan University, Shanghai 200433, China

S *Supporting Information*

ABSTRACT: In recent years, self-assembly of block or graft copolymers with sugar-containing component has drawn great attention. We just reported that protection−deprotection chemistry could initiate self-assembly of glycopolymers based on the high polarity change induced by the deprotection. Considering that the protection−deprotection is so common and its variety in glycochemistry, it is worth developing this finding into a new and general strategy of self-assembly of glyco-containing polymers. For this purpose, this article focuses on the kinetics and morphology control of the assemblies of glyco-block copolymers induced by the deprotection. Benzoyl (**Bz**) as the protective group was introduced, which has much lower deprotection rate than acetyl group (**Ac**) reported previously. Thus, the detailed kinetic study of the self-assembly of **Bz** copolymer by means of *in situ* light scattering and ^{1}H NMR, etc., became possible. The morphologies of all of the resultant assemblies were observed by cryo-TEM. Thus, we found that in the case of using an equivalent catalyst TBAOH, with the progress of deprotection of **Bz**, the copolymer follows three-stage assembly, i.e., fast initiation, steady growth, and then fission/reorganization into stable state. In most conditions, both **Bz** and **Ac** copolymers form stable vesicles, but the former is apparently larger than the latter. This is because that the slow deprotection of **Bz** makes the resultant assemblies assume structures closer to equilibrium, and the fast reaction of **Ac** makes the assemblies with more kinetic-trapped features.

INTRODUCTION

Self-assembly of block copolymers containing bioactive species, including peptides and sugars, has attracted more and more attention due to their role in deepening one's understanding of the related processes in living systems and the promising potential applications in biomedicine.[1] However, until now, the common strategies to self-assemble these biocopolymers in solution have been limited. In the most common way, the peptide/sugar-based blocks play the role of a hydrophilic block to stabilize the obtained nanostructures in the self-assembly processes which are induced by the hydrophobicity or responsiveness of the other non-bio-block.[2−7] Obviously, the limitation on self-assembly strategy of glycopolymers slowed down our footsteps on the exploration of new sweet materials in biomedicine. Thus, it is demanding to develop new self-assembly strategies. It is known that monosaccharides and oligosaccharides are aldehydes or ketones with multiple hydroxyl groups, which always interfere the reactions in

preparation of the related monomers and polymers. Fortunately, the protection−deprotection process developed in glycochemistry succeeds in eliminating such interference. Accompanying the deprotection, i.e., removal of the protective groups, a significant polarity change of the glyco-block takes place. However, the possible role of such change in self-assemble of glyco-block-containing copolymers was neglected. Recently, we first proposed and realized the protection−deprotection strategy for self-assembly of a glyco-block-containing copolymer leading to glyco-inside vesicles and micelles.[8]

This deprotection-induced micellization can be regarded as a significant advance of self-assembly of block copolymer induced by chemical reactions. In this field, there are some well-known
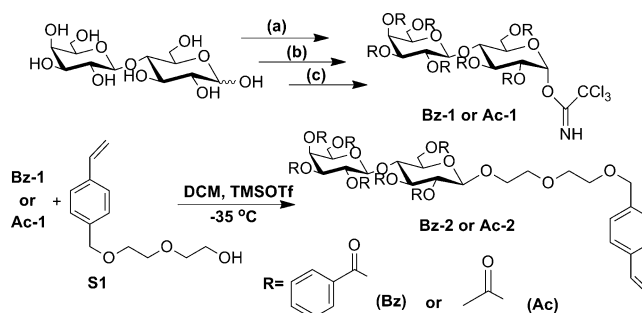
 A

examples; chemical reaction-induced self-assembly of copolymer chain of poly(phenylvinyl sulfoxide) (PVSO) and poly(4-methylstyrene) (PMS) was first reported several years ago.[9] Recently, for block copolymers consisting of a polystyrene (PS) block and a photocleavable block, Gohy et al.[10] realized its micellization by the cleavage of O-nitrobenzyl esters. Compared to the chemical interactions used in such examples, the protection−deprotection is much more general and in some extent indispensable in glycochemistry. Moreover, the well-established carbohydrate chemistry provides many kinds of protective groups with similar functionality but different reactivity. So a broader scope of chemistry is available for developing this macromolecular self-assembly. Therefore, the strategy induced by this reaction is worth exploring more extensively. On the basis of our previous exploration, in this paper, we will introduce benzoyl (**Bz**) group to well-characterized glycomonomer and glycopolymer. The self-assembly of the latter will be induced by deprotection of the **Bz** moiety. Strikingly, we found that starting from very similar backbone removal of **Bz** group and acetyl (**Ac**) group induces very different self-assembly kinetics and even different self-assembled morphologies.

■ RESULTS AND DISCUSSION

Design and Synthesis of Benzoyl-Containing Monomer and Copolymers. In our previous study, **Ac** was employed as the protective group to control the self-assembly of glycopolymers.[8] However, the **Ac** removal was so fast that the corresponding self-assembly process could not be monitored. In current research for exploring how is the assembly directed by the deprotection chemistry, we tried to find some other esters with moderate reactivity first. Thus, model deprotection reactions on two disaccharides (**S3** and **S5**, Supporting Information) protected with benzoyl and acetyl, respectively, were performed by using tetrabutylammonium hydroxide (TBAOH), which was proved powerful to remove **Ac** groups on polymer side chain in our previous study.[8] As in the reaction TBAOH forms equivalent (n-$C_4H_9)_4N^+C_6H_5COO^-$ for **Bz**, which will be discussed later; strictly speaking, it serves a reactant rather than a catalyst. For clarity, the number of equivalency of TBAOH used in this paper is calculated according to the molar amount of protective groups. As shown in Figure S1, TLC results showed that 2.5 equiv of TBAOH to **Bz** or **Ac** groups was capable to remove all of the protective groups but the **Bz** removal was finished in 10 min while **Ac** in 5 min. Furthermore, 1.0 equiv amount of TBAOH could remove all of **Ac** groups in about 15 min, but only part of **Bz** groups could be removed even in much longer time. This result of comparing the deprotection rate between **Bz** and **Ac** is generally in agreement with that reported in the literature,[11] indicating that the **Bz** group could be a good candidate for the kinetic study of the self-assembly of glycopolymers.

To compare the self-assembly behavior of **Bz**- and **Ac**-protected glycopolymers, the corresponding monomers were designed first. As shown in Scheme 1, glycosylation donors **Bz-1** and **Ac-1** were prepared via three steps according the reaction conditions reported in the literature.[12] After glycosylation reaction with the same acceptor **S1**, the vinyl group was successfully coupled to **Bz-1** and **Ac-1**, generating new monomers **Bz-2** and **Ac-2**. ^{1}H NMR and ^{13}C NMR characterization of the two monomers are shown in Figure 1 and Figure S2, respectively. Synthetic details and character-

Scheme 1. Synthetic Route of Lactopyranomonomers Bz-2 and Ac-2 with Bz and Ac Protection, Respectively[a]

[a]Reagents: (a) benzoyl chloride, 4-(dimethylamino)pyridine (DMAP), triethylamine (TEA); (b) hydrazine acetate, N,N-dimethylformamide (DMF); (c) 1,8-diazabicyclo[5.4.0]undec-7-ene (DBU), trichloroacetonitrile, dichloromethane (DCM); TMSOTf: trimethylsilyl trifluoromethanesulfonate.

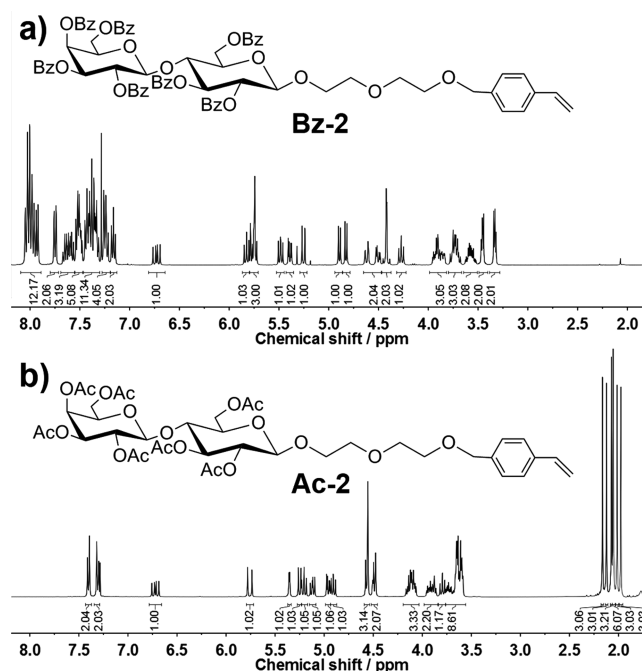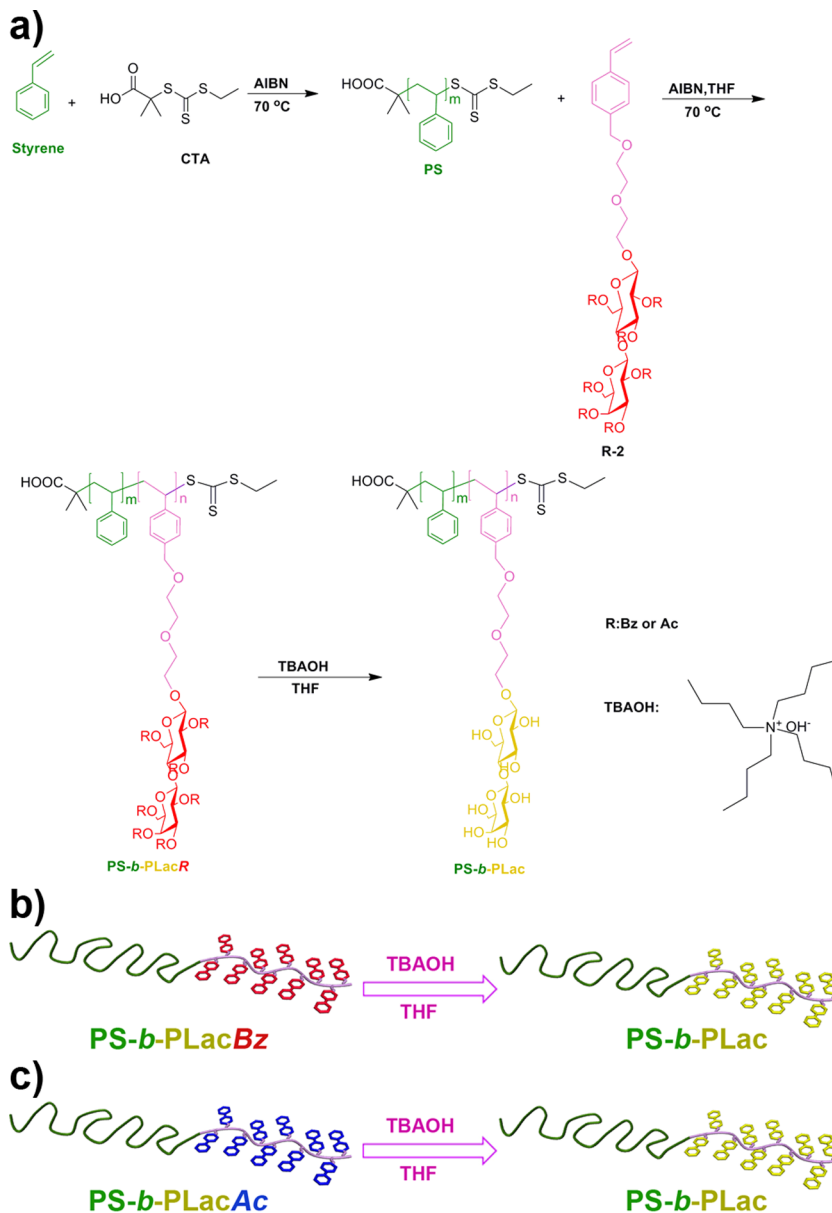ization on the intermediates and monomers are shown in the Supporting Information (Scheme S1).

Figure 1. ^{1}H NMR spectra of monomers (a) **Bz-2** and (b) **Ac-2**.

Reversible addition−fragmentation chain transfer (RAFT) polymerization on monomer **Bz-2** and **Ac-2** was performed with the RAFT macro chain transfer reagent (macroCTA) **PS** (Scheme 2) in bulk at 70 °C. To each monomer, two copolymers were synthesized with the same macroCTA, but different degree of polymerization (DP) of glyco-monomers. The polymerization was proved to be successful as the products showed unimodal gel permeation chromatography (GPC) curves in Figure 2 and the calculated polydispersity (PDI) was low, around 1.2 (Table 1). As the chemical structure of our glyco-block is very different from the PS standard in GPC measurements, large errors in calculating molecular weight are expected. So more believable molecular weights from GPC-MALS, where absolute molecular weight was measured by multiangle light-scattering (MALS) detector, are listed in Table

Scheme 2. Synthetic Route of Glycopolymers PS-*b*-PLac*R* and the Deprotection To Form PS-*b*-PLac by Using TBAOH[a]

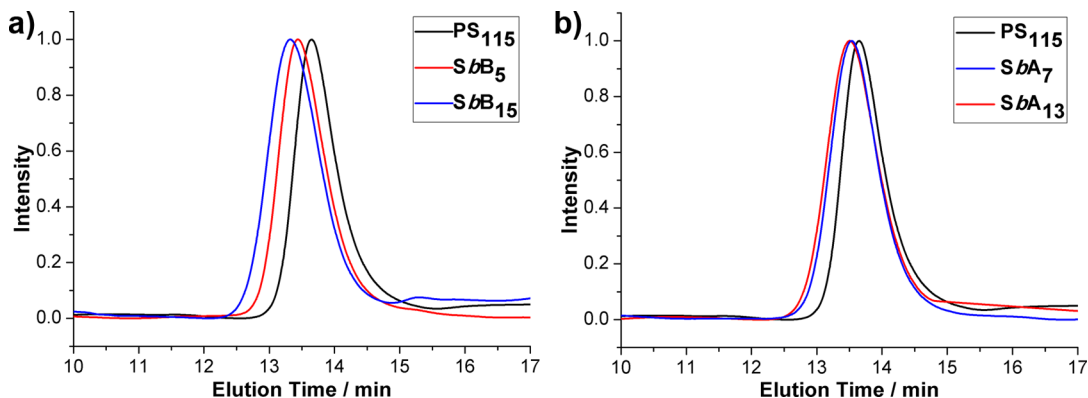[a] Red for the lactopyranoside protected by **Bz**, blue for protected by **Ac**, and yellow for unprotected **Lac**.

Figure 2. GPC curves of (a) **S*b*B$_5$**, **S*b*B$_{15}$** and (b) **S*b*A$_7$**, **S*b*A$_{13}$** and the corresponding macro-CTA **PS$_{115}$** in DMF.

1. Meanwhile, the number-average molecular weight (M_n) from ^{1}H NMR in Table 1 could be in a large error as the designed length of glyco-block was quite short compared to that of **PS** block. Table 1 lists the characterization data of four copolymers,

Table 1. Molecular Weight Characterization on Copolymers Used in Deprotection Study by ^{1}H NMR, GPC, and GPC-MALS

		^{1}H NMR	GPC-MALS[b]	GPC[c]			
code	copolymer	M_n	M_w	M_w	M_n	PDI	ratio[d]
	PS$_{115}$	12200	12200	10700	8900	1.20	0
SbB$_5$	PS$_{115}$-b-PLacBz$_5$	a	19300	15800	13100	1.21	0.23
SbB$_{15}$	PS$_{115}$-b-PLacBz$_{15}$	a	34000	19000	15700	1.21	0.68
SbA$_7$	PS$_{115}$-b-PLacAc$_7$	18000	18050	16600	14000	1.19	0.32
SbA$_{13}$	PS$_{115}$-b-PLacAc$_{13}$	23100	27610	19700	16300	1.21	0.59

[a]Could not be measured due to low solubility. [b]M_w measured from GPC-MALS. [c]M_n, M_w, and PDI were calculated from GPC with PS as standard. [d]Calculated from the weight ratio of sugar block to PS block after deprotection.
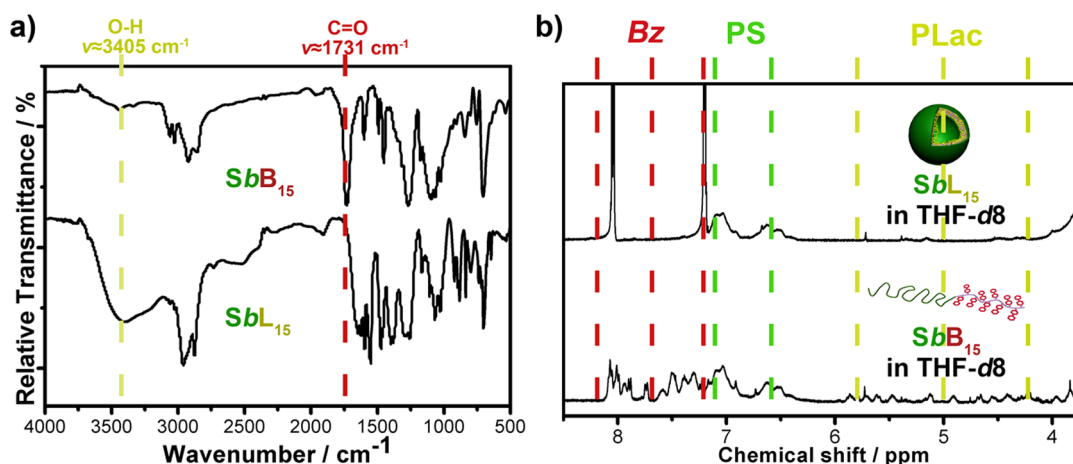

Figure 3. (a) FT-IR spectra and (b) ^{1}H NMR of **SbB$_{15}$** and **SbL$_{15}$**. For FT-IR, after 10 min reaction and dialysis against water, the resultant powder of the deprotected product was collected and used for the measurement.

i.e., **PS$_{115}$-b-PLacBz$_{15}$**, **PS$_{115}$-b-PLacAc$_{13}$**, and **PS$_{115}$-b-PLacBz$_5$**, **PS$_{115}$-b-PLacAc$_7$**, where **Lac** represents the glyco-block with disaccharide pendent group of lactopyranoside. For clarity, the four copolymers are represented as **SbB$_{15}$**, **SbA$_{13}$**, **SbB$_5$**, and **SbA$_7$**, respectively; accordingly, after being completely deprotected, the four copolymers are called **SbL$_{15}$**, **SbL$_{13}$**, **SbL$_5$**, and **SbL$_7$**. Details of the molecular weight measurements are listed in the Supporting Information (Figures S3−S15). Thus, we have two pairs of the copolymers. In each pair, the **Bz** and **Ac** moieties have very similar DP values. We found that all the four block copolymers could be molecularly dissolved in THF by DLS measurements shown in Figure S17.

Analysis on Deprotection of Copolymers by FT-IR and ^{1}H NMR. Deprotection reaction on the copolymers containing **Bz**-protected disaccharides was studied by Fourier transform infrared spectroscopy (FT-IR) and ^{1}H NMR first. Deprotection of **SbB$_{15}$** (1.25 mg/mL in THF) was performed by addition of an excess, i.e., 2.5 equiv of aqueous TBAOH (10 μL, 40 wt %). As shown in Figure 3a, compared to the FT-IR spectrum of **SbB$_{15}$**, the resultant copolymer showed complete disappearance of the signal belonging to **Bz** groups at 1731 cm^{-1} (ν(C=O)) and a great enhancement of the characteristic broad absorption of hydroxyl groups at 3405 cm^{-1} (Figure 3a) as well, demonstrating the successful removal of **Bz** groups and formation of unprotected **SbL$_{15}$**. ^{1}H NMR was then employed to confirm this process (Figure 3b). For the spectra of **SbB$_{15}$**, the peaks around δ 6.00−4.00 ppm belonged to the protons on the pyranose ring of lactose, and those around δ 7.16−6.30 ppm showed the phenyl groups directly bonded to the polymeric backbone. In addition, the peaks around δ 8.30−

7.16 ppm were assigned to the protons of **Bz** groups. Clearly, after the reaction, the peaks associated with **Bz** completely disappeared as a result of the full deprotection. However, the peaks belonging to the protons of lactopyranoside disappeared as well. This indicated that due to the solvophobicity of the exposed hydroxyl groups of lactose in THF, the resultant copolymer self-assembled into nanoparticles with glyco-inside structure. In addition, it was worth noting that the peaks around δ = 8.05 ppm and δ = 7.20 ppm generated after deprotection were found to be associated with the soluble structure of $(n\text{-}C_4H_9)_4N^+C_6H_5COO^-$, which was confirmed by ESI-MS (Figure S16). This means that **TBAOH** in fact reacted with the **Bz** group equivalently. In short, combining the results for **Bz** copolymers mentioned above and that for **Ac** copolymers (Figure S18), we could conclude that both **Bz** or **Ac** groups on the copolymer in THF could be removed with an excess amount of TBAOH, and the deprotection reaction induced their self-assembly to nanostructures with glyco-block inside.

Self-Assembly of Bz and Ac Copolymers with an Excess of Catalyst. In this section we discuss and compare the self-assembly of the block copolymers with an excess of TBAOH; i.e., the relative molar ratios of TBAOH to **Bz** and **Ac** groups were 2.5 and 2.1, respectively. As shown in Figure 4a, for both **Bz** and **Ac** copolymers, upon addition of TBAOH, the average hydrodynamic radius $\langle R_h \rangle$ of the copolymer solution in THF measured by dynamic light scattering (DLS) increased very fast at first until reaching a plateau where the $\langle R_h \rangle$ no longer changed, indicating formation of stable nanostructures, which were named **V-Bz-3** from **SbB$_{15}$** and **V-Ac-3** from **SbA$_{13}$**. The results indicated that the self-assembly of both the **Bz** and **Ac** copolymers follow the similar process. However, the
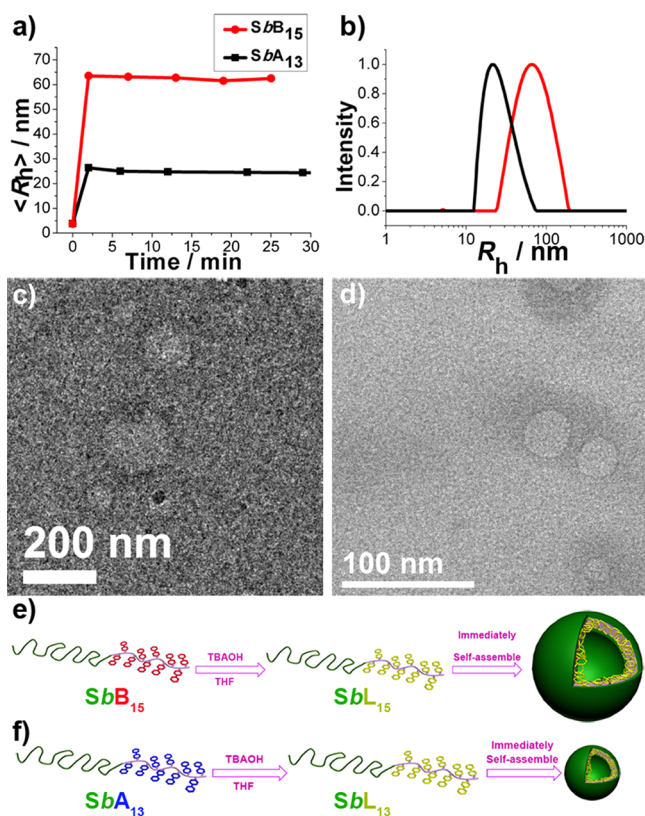
Figure 4. (a) Evolution of $\langle R_h \rangle$ during the self-assembly process started from addition of excess amount of TBAOH (40 wt %, 10 μL) into the THF solution of **SbB$_{15}$** and **SbA$_{13}$** (1.5 mL, 1.25 mg/mL). (b) R_h distribution of **V-Bz-3** and **V-Ac-3**. Cryo-TEM images of (c) **V-Bz-3** and (d) **V-Ac-3**. Cartoon scheme of self-assembly of (e) **SbB$_{15}$** and (f) **SbA$_{13}$**.

resultant assemblies are quite different in size: as shown in Figure 4a,b, $\langle R_h \rangle$ of **V-Bz-3** was around 58 nm, while that of **V-Ac-3** was only around 24 nm. Under cryogenic transmission electron microscopy (cryo-TEM), both of the stabilized nanostructures showed vesicular morphology but quite different diameters in consistent to the results from DLS. Moreover, the vesicle morphology was also supported by the values of $\langle R_g \rangle / \langle R_h \rangle$, where $\langle R_g \rangle$ was obtained from static light scattering (SLS), shown in Table 2. The number of aggregation (N_{agg}) of 935 for **V-Bz-3** and 166 for **V-Ac-3** calculated from SLS also showed an apparent difference.

The apparent difference in size between **V-Bz-3** and **V-Ac-3** was unexpected as here an excess of catalyst was used capable of removing all the protective groups, and therefore the resultant copolymers from **Bz** and **Ac** copolymers should be the same in chemistry. This difference clearly demonstrates the role of process and kinetics of deprotection on the final size and morphology. Although we could not follow the assembly process in details by DLS for so quick process, it is reasonable to think that **Ac** removal is so fast that the assembly structure

could be formed and frozen soon after addition of TBAOH, and therefore formation of larger aggregates which required more block molecules to get together by diffusion became almost impossible. In contrast, **Bz** removal proceeded slower, which enabled the copolymer molecules to have chance to adjust their conformation and diffuse to close to each other forming vesicles with a size close to its equilibrium structure. In addition, it seems not surprising to find that for the current copolymers with the low ratio of the unit number of the solvophobic block (**Bz$_{15}$** and **Ac$_{13}$**) to the solvophilic block (**PS$_{115}$**) forming vesicles instead of micelles, if the much larger volume of the sugar repeating unit than that of PS unit is considered.[8]

Self-assembly of the second pair of copolymers with the shorter glyco-block, i.e., **SbB$_5$** and **SbA$_7$**, by addition of excess of TBAOH (13.3 μL, 4.0 equiv) in THF solutions (1.5 mL, 1.25 mg/mL) was performed as well. Full removal of **Bz** and **Ac** group of the copolymers was proved by FT-IR and ^{1}H NMR as shown in Figures S19 and S20. Kinetic behavior of the assembly for this pair was very similar to the pair with long **Bz** and **Ac** blocks just discussed; i.e., the $\langle R_h \rangle$ increased very fast at first and then remained stable (Figure 5a,b). However, as revealed by cryo-TEM, the deprotection of **SbB$_5$** led to vesicles (**V-Bz-4**) while **SbA$_7$** led to micelles (**M-Ac-4**) (Figure 5c,d). The size difference between them was also striking, i.e. $\langle R_h \rangle$ of **V-Bz-4** was around 140 nm, while that of **M-Ac-4** was only around 14 nm. Similar with the above discussion for the pair of copolymers with the long glyco-block, here the different deprotection rate between **Bz** and **Ac** was attributed to the apparent difference of the resultant assemblies because the assemblies from **Bz** and **Ac** copolymers are in fact in different degrees of kinetically trapped structures (Figure 5e,f).

Self-Assembly with Equivalent Catalyst. For the case of using an excess catalyst, even for **Bz** copolymers with relatively slow deprotection rate, the detail process of the assembly still could not be followed by any available techniques. Therefore, here an equivalent TBAOH was used to the solution of **SbB$_{15}$** and **SbA$_{13}$** (1.25 mg/mL) in THF. As shown in Figure 6a, when 1.0 equiv of TBAOH (8 μL, 20 wt %) was added into the THF solution of **SbB$_{15}$**, it showed very different kinetics: $\langle R_h \rangle$ of the solution suddenly increased to 120 nm within 5 min (stage I) followed by a slow increase (in about 45 min, stage II) until a maximum value ($\langle R_h \rangle$ = 270 nm) reached. Then $\langle R_h \rangle$ began to quickly decrease to and kept stable around 50 nm within 15 min (stage III) forming the final stable nanostructure **V-Bz-5**. By contrast, for **SbA$_{13}$**, even only 1.0 equiv of TBAOH (8 μL, 24 wt %) was used, the kinetic character was the same as that for the excess catalyst: rapid formation of nanoparticles (**V-Ac-5**, $\langle R_h \rangle$ = 22 nm) was observed, which became stable over a long time. Moreover, cryo-TEM images proved the vesicle morphology for the both (Figure 6b,c). And the $\langle R_g \rangle / \langle R_h \rangle$ values of **V-Bz-5** and **V-Ac-5** were found to be 1.12 and 1.17 (Table 3), respectively, confirming their vesicular structure. But **V-Bz-5** was much larger than that of **V-Ac-5** in weight; i.e., the number of aggregation (N_{agg}) calculated from SLS of the

Table 2. Summary of $\langle R_h \rangle$, PDI, and Morphology of the Self-Assembled Structures in THF^a

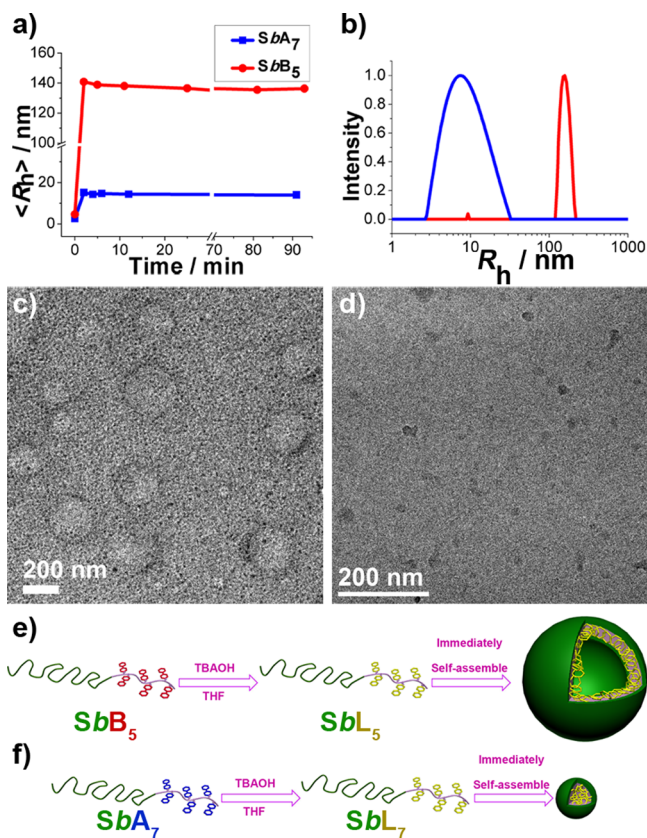| starting copolymer	particle	TBAOH (equiv)	$\langle R_h \rangle$ (nm)	PDI	$\langle R_g \rangle$ (nm)	$\langle R_g \rangle / \langle R_h \rangle$	N_{agg}	morphology
SbB$_{15}$	**V-Bz-3**	2.5	58	0.11	63	1.09	935	vesicle
SbA$_{13}$	**V-Ac-3**	2.1	24	0.13	29	1.21	166	vesicle

^{a}Data were collected by DLS and SLS.

E

Figure 5. (a) Evolution of $\langle R_h \rangle$ during the self-assembly process started from addition of TBAOH (13.3 μL, 4.0 equiv) into the solution of **SbB$_5$** and **SbA$_7$** (1.5 mL, 1.25 mg/mL) in THF. (b) R_h distribution of **V-Bz-4** and **M-Ac-4**. The cryo-TEM images of (c) **V-Bz-4** and (d) **M-Ac-4**. Cartoon scheme of self-assembly of (e) **SbB$_5$** and (f) **SbA$_7$**.

former was 841, while that of the latter was only 146. Moreover, the compositions of resulting vesicles were slightly different; i.e., as shown in Figure S21, only a tiny amount of **Ac** groups remained after deprotection, while more **Bz** groups did so on the copolymer chain as demonstrated in Figure S22, which will be discussed in detail below.

The complex kinetics of **SbB$_{15}$** with an equivalent catalyst was further studied in detail. The results from three groups of experiments are shown in Figure 7, where the same amount of aqueous TBAOH (1.0 equiv) in different concentrations and also with different amounts of water, i.e. 40 wt %, 4 μL; 20 wt %, 8 μL; and 10 wt %, 16 μL (the middle case was just mentioned) were added to the THF solution of **SbB$_{15}$** (1.5 mL,

1.25 mg/mL). As shown in Figure 7, the three groups show the same kinetic characters: the $\langle R_h \rangle$ evolution follows the three-stage pathway, i.e., fast initiation, steady growth to a turning point, and then fast decrease to stable state. The corresponding evolution of the R_h distribution profiles during the deprotection shown in Figure 7d−f provided more information about the assembly process: an abrupt right shift of the peak was observed soon after addition of TBAOH, and then the peak shifted slowly. These changes obviously correspond to the initial fast and the slow increase of $\langle R_h \rangle$ value. Afterward, when $\langle R_h \rangle$ reached the turning point in Figure 7a−c, in the profiles, a small peak at a low R_h value appeared leading to a bimodal distribution of R_h (Figure 7d−f). Then the bimodal distribution went back to unimodal one with the peak at the smaller R_h value. So in the stage III, what happening could be fission of the large aggregates and reorganization, which finally resulted in smaller but stable aggregates. Furthermore, all the final three stable structures were found to be vesicles (Figure 7g−i and Table 4).

Meanwhile, removal of **Bz** group from the glyco-block was monitored by ^{1}H NMR during the whole deprotection process (Figures S23−S25). After addition of TBAOH, a sharp peak appeared around δ = 7.20 ppm associated with the removed **Bz** group of $(n\text{-}C_4H_9)_4N^+C_6H_5COO^-$, which was quantified via internal standard tetraethylsilane and used as an indicator of the degree of deprotection. Fully deprotected **SbB$_{15}$** was first generated to give the possible total amount of free **Bz** peaks. As shown in Figure 7a−c, generally, there is a fast initial removal followed by a slow process, which generally corresponded to the stage I and II of the assembly, respectively. So the results clearly indicated that the assembly was driven by the deprotection. It is interesting to find that the aggregation in fact was initiated very soon after the catalyst was added where the great amount of **Bz** groups still remained. So at this stage the aggregation force due to the solvophobic character of the resultant hydroxyl groups is not enough to form stable assemblies. With increasing amount of removed **Bz** groups, the aggregates grew to quite larger size around 200−400 nm depending on the water amount added. Such large size was far beyond the expected equilibrium values, so they were believed to be loose and kinetically trapped aggregates. This opinion found support from the morphology observation of the samples collected from the solution at the stage I and stage II, respectively, as being arrowed in Figure 7a. As shown in Figure 8b,c, the TEM images of both do not show any regular structure of self-assemblies but just irregular aggregates. Afterward, these unstable aggregates further fissioned and reorganized into stable vesicles when the deprotection proceeded slowly (Figure 8a).
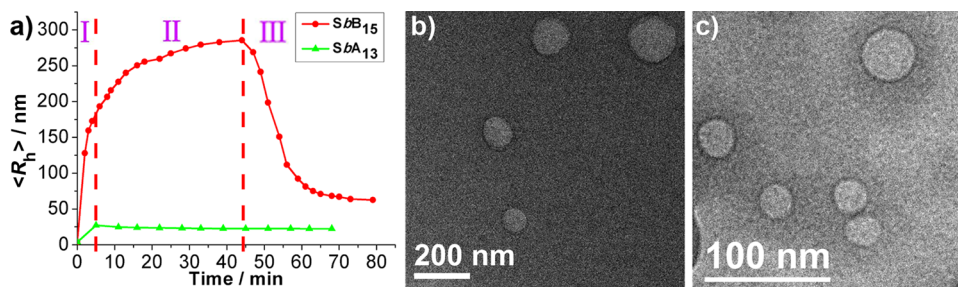

Figure 6. (a) Evolution of $\langle R_h \rangle$ during the self-assembly process starting from addition of 8.0 μL of TBAOH (1.0 equiv) into the THF solution of **SbB$_{15}$** (red line) and **SbA$_{13}$** (green line) (1.5 mL, 1.25 mg/mL). The cryo-TEM images of (b) **V-Bz-5** and (c) **V-Ac-5**.

Table 3. Summary of $\langle R_h \rangle$, PDI, and Morphology of the Self-Assembled Structures in THF^a

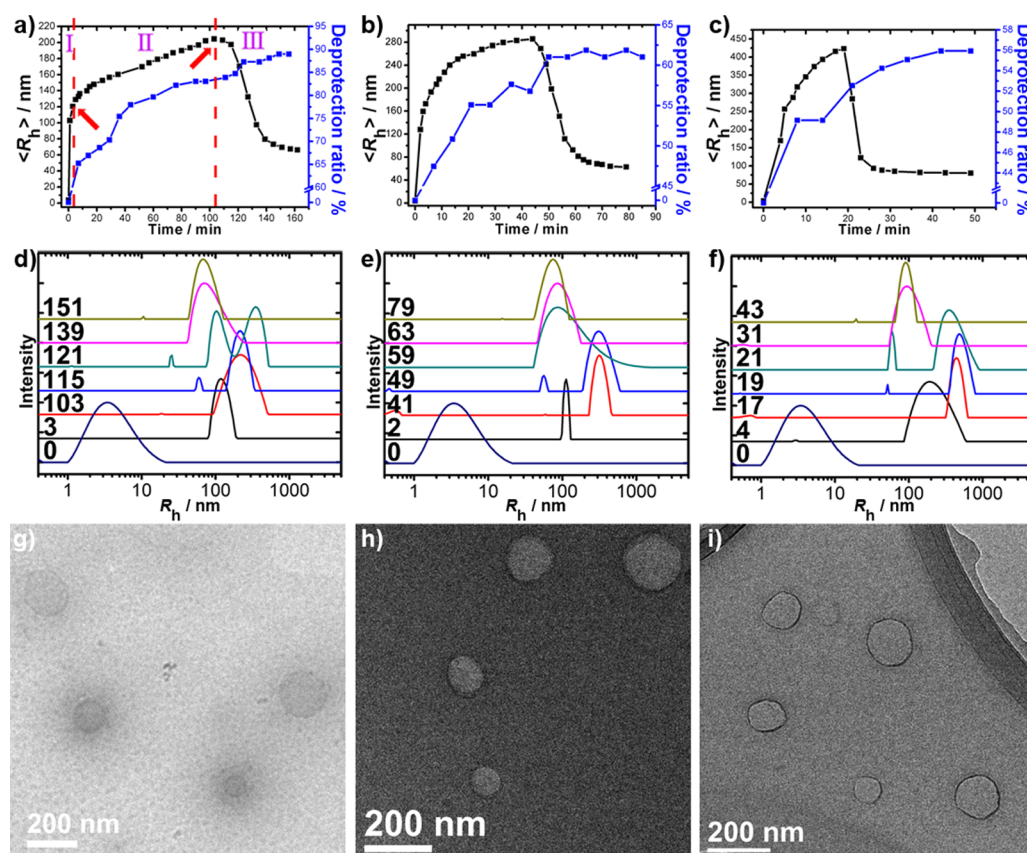| starting copolymer	particle	TBAOH (equiv)	$\langle R_h \rangle$ (nm)	PDI	$\langle R_g \rangle$ (nm)	$\langle R_g \rangle / \langle R_h \rangle$	N_{agg}	morphology
SbB_{15}	V-Bz-5	1.0	57	0.06	64	1.12	841	vesicle
SbA_{13}	V-Ac-5	1.0	23	0.13	27	1.17	146	vesicle

^{a}Data were collected by DLS and SLS.

Figure 7. Evolution of $\langle R_h \rangle$ (black line) and degree of deprotection (%, blue line) calculated from the peaks around $\delta = 7.20$ ppm in ^{1}H NMR during the self-assembly process by addition of (a) 4 μL of TBAOH (40 wt %), (b) 8 μL of TBAOH (20 wt %), and (c) 16 μL of TBAOH (10 wt %) into the THF solution of SbB_{15} (1.5 mL, 1.25 mg/mL). Corresponding R_h distribution changes (d, e, f) and cryo-TEM images of the stable self-assembled structures (g, h, i). (a, d, g; b, e, h; and c, f, i are for the respective same conditions).

Table 4. Summary of $\langle R_h \rangle$, PDI, and Morphology of the Self-Assembled Structures in THF^a

starting copolymer	particle	TBAOH		$\langle R_h \rangle$ (nm)	PDI	$\langle R_g \rangle$ (nm)	$\langle R_g \rangle / \langle R_h \rangle$	N_{agg}
		μL	wt %					
SbB_{15}	V-Bz-6	4	40	52	0.09	60	1.17	740
$SbB_{15}{}^b$	V-Bz-5	8	20	57	0.06	64	1.12	841
SbB_{15}	V-Bz-7	16	10	84	0.10	94	1.12	2060

^{a}Data were collected by DLS and SLS. ^{b}The same as Table 3.

Comparing the three groups, it was clear that the larger amount of water, the faster the assemblies reached the maxium $\langle R_h \rangle$ (100, 45, and 20 min for 4, 8, and 16 μL aqueous solution of TBAOH, respectively), then faster turned to the stable state. It seemed understandable as the small amount water served cocatalyst accelerating the deprotection. Moreover, the final degree of deprotection varied with the amount of water used, i.e., 90%, 60%, and 55% removal of **Bz** for 4, 8, and 16 μL aqueous TBAOH, respectively. The corresponding $\langle R_h \rangle$ of the final vesicles were 52 nm (**V-Bz-6**), 57 nm (**V-Bz-5**), and 84 nm (**V-Bz-7**). This means that as the larger amount of the **Bz** group remained on the copolymer, the larger the solvent-phobicity, and consequently the larger the vesicles generated.

CONCLUSIONS

In this paper, removal of **Bz** group has been used to induce self-assembly of glyco-*block*-containing copolymers for the first time. Compared to **Ac** group, the slower deprotection speed of **Bz** brought much more space and variations, which makes the detail studies of kinetics and morphology control of the deprotection-induced self-assembly possible. After careful analysis on the data from DLS, SLS, *in situ* NMR, and cryo-TEM, etc., we found that **Bz** removal always gave much larger
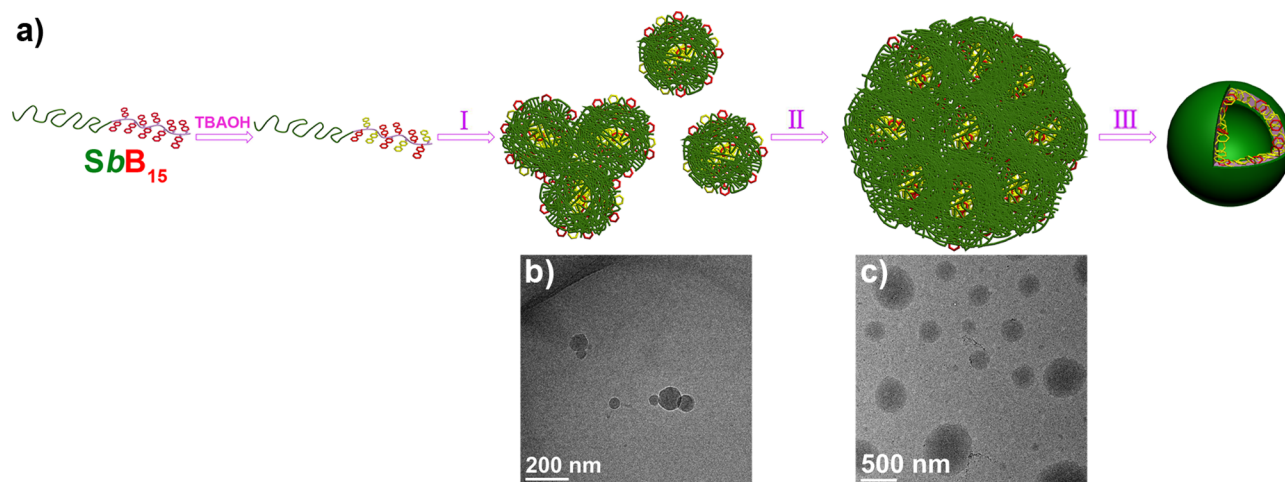
Figure 8. (a) Proposed mechanism of the assembly process in Figure 7a. Cryo-TEM images of the assemblies collected at (b) state I and (c) state II as arrowed in Figure 7a.

size of the vesicles than **Ac** removal, which could be explained as the slower deprotection leading to more thermodynamic-controlled morphology, while the fast deprotection generating kinetics-controlled morphology. Accompanying the deprotection of **Bz**, three-state evolution was observed, i.e., fast formation of unstable micelles, micelle growth, and then fission/reorganization into stable vesicles. In short, this work shows the power of the deprotection reaction on controlling the self-assembly process and morphology of the obtained nanostructures. Considering the existing library of protective groups with similar functionality in carbohydrate chemistry, a bright future of this new strategy can be predicted.

■ ASSOCIATED CONTENT

Ⓢ Supporting Information

Synthesis and characterization of monomer **Bz-2** and **Ac-2**, block copolymer **SbB$_{15}$, SbB$_5$, SbA$_{13}$,** and **SbA$_7$,** including ^{1}H NMR as well as details of GPC-MALS, FT-IR, and SLS measurements. The Supporting Information is available free of charge on the ACS Publications website at DOI: 10.1021/acs.macromol.5b00572.

■ AUTHOR INFORMATION

Corresponding Author
*E-mail guosong@fudan.edu.cn; Tel +86 21 55664275 (G.C.).

Notes
The authors declare no competing financial interest.

■ ACKNOWLEDGMENTS

■ REFERENCES

(1) (a) Becer, C. R.; Gibson, M. I.; Geng, J.; Ilyas, R.; Wallis, R.; Mitchell, D. A.; Haddleton, D. M. *J. Am. Chem. Soc.* **2010**, *132*, 15130−15132. (b) Huang, J.; Bonduelle, C.; Thévenot, J.; Lecommandoux, S.; Heise, A. *J. Am. Chem. Soc.* **2012**, *134*, 119−122. (c) Zhou, C.; Wang, M.; Zou, K.; Chen, J.; Zhu, Y.; Du, J. *ACS Macro Lett.* **2013**, *2*, 1021−1025. (d) Hu, X.; Hu, J.; Tian, J.; Ge, Z.; Zhang, G.; Luo, K.; Liu, S. *J. Am. Chem. Soc.* **2013**, *135*, 17617−17629.
(2) Narain, R.; Armes, S. P. *Biomacromolecules* **2003**, *4*, 1746−1758.
(3) Becer, C. R.; Babiuch, K.; Pilz, D.; Hornig, S.; Heinze, T.; Gottschaldt, M.; Schubert, U. S. *Macromolecules* **2009**, *42*, 2387−2394.
(4) (a) Su, L.; Zhao, Y.; Chen, G.; Jiang, M. *Polym. Chem.* **2012**, *3*, 1560−1566. (b) Sun, P.; He, Y.; Lin, M.; Zhao, Y.; Ding, Y.; Chen, G.; Jiang, M. *ACS Macro Lett.* **2013**, *3*, 96−101.
(5) Zhang, Q.; Wilson, P.; Anastasaki, A.; McHale, R.; Haddleton, D. M. *ACS Macro Lett.* **2014**, *3*, 491−495.
(6) (a) You, L.; Schlaad, H. *J. Am. Chem. Soc.* **2006**, *128*, 13336−13337. (b) Schlaad, H.; You, L.; Sigel, R.; Smarsly, B.; Heydenreich, M.; Mantion, A.; Masic, A. *Chem. Commun.* **2009**, 1478−1480.
(7) Ladmiral, V.; Semsarilar, M.; Canton, I.; Armes, S. P. *J. Am. Chem. Soc.* **2013**, *135*, 13574−13581.
(8) Su, L.; Wang, C.; Polzer, F.; Lu, Y.; Chen, G.; Jiang, M. *ACS Macro Lett.* **2014**, *3*, 534−539.
(9) Wu, C.; Niu, A.; Leung, L. M.; Lam, T. S. *J. Am. Chem. Soc.* **1999**, *121*, 1954−1955.
(10) (a) Gohy, J.-F.; Zhao, Y. *Chem. Soc. Rev.* **2013**, *42*, 7117−7129. (b) Bertrand, O.; Schumers, J.-M.; Kuppan, C.; Marchand-Brynaert, J.; Fustin, C.-A.; Gohy, J.-F. *Soft Matter* **2011**, *7*, 6891−6896. (c) Schumers, J.-M.; Bertrand, O.; Fustin, C.-A.; Gohy, J.-F. *J. Polym. Sci., Part A: Polym. Chem.* **2012**, *50*, 599−608.
(11) (a) Yao-Chang, X.; Bizuneh, A.; Walker, C. *Tetrahedron Lett.* **1996**, *37*, 455−458. (b) Lee, J.-C.; Chang, S.-W.; Liao, C.-C.; Chi, F.-C.; Chen, C.-S.; Wen, Y.-S.; Wang, C.-C.; Kulkarni, S. S.; Puranik, R.; Liu, Y.-H.; Hung, S.-C. *Chem.—Eur. J.* **2004**, *10*, 399−415. (c) Chung, S.-K.; Yu, S.-H. *Bioorg. Med. Chem. Lett.* **1996**, *6*, 1461−1464. (d) Sureshan, K. M.; Shashidhar, M. S.; Praveen, T.; Das, T. *Chem. Rev.* **2003**, *103*, 4477−4504.
(12) (a) Sandbhor, M. S.; Soya, N.; Albohy, A.; Zheng, R. B.; Cartmell, J.; Bundle, D. R.; Klassen, J. S.; Cairo, C. W. *Biochemistry* **2011**, *50*, 6753−6762. (b) Khan, S. N.; Kim, A.; Grubbs, R. H.; Kwon, Y.-U. *Org. Lett.* **2012**, *14*, 2952−2955. (c) Kale, R. R.; Clancy, C. M.; Vermillion, R. M.; Johnson, E. A.; Iyer, S. S. *Bioorg. Med. Chem. Lett.* **2007**, *17*, 2459−2464. (d) Beckmann, H. S. G.; Niederwieser, A.; Wiessler, M.; Wittmann, V. *Chem.—Eur. J.* **2012**, *18*, 6548−6554. (e) Zhang, X.-R.; Jia, J.-L.; Zhang, R.-J.; Xu, M.-H.; Zhang, S.-S. *Chin. J. Chem.* **2006**, *24*, 1058−1061.